

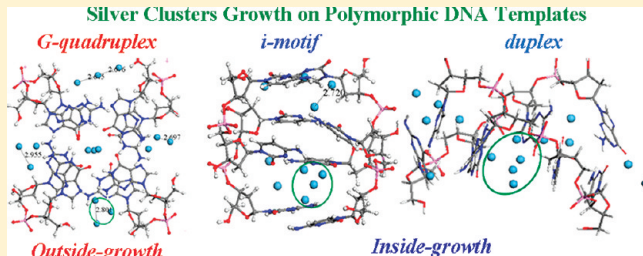
# Growth Mechanisms of Fluorescent Silver Clusters Regulated by Polymorphic DNA Templates: A DFT Study

Jiangjiexing Wu,<sup>†</sup> Yan Fu,<sup>‡</sup> Zhenghua He,<sup>†</sup> You Han,<sup>†</sup> Lin Zheng,<sup>†</sup> Jinli Zhang,<sup>‡</sup> and Wei Li\*,<sup>†</sup>

<sup>†</sup>Key Laboratory for Green Chemical Technology MOE and <sup>‡</sup>Key Laboratory of Systems Bioengineering MOE, Tianjin University, Tianjin 300072, People's Republic of China

Supporting Information

**ABSTRACT:** The aggregation behaviors of silver atoms modulated by polymorphic DNA templates involving i-motif, G-quadruplex, and the Watson–Crick duplex, were investigated by using the density functional theory (DFT) calculations, combining with the experimental characterizations of CD, UV, fluorescence measurements and TEM, in order to understand the reason in the molecular level that polymorphic DNA templates affect the fluorescence emitting species of Ag nanomaterials. First, the affinity sites of silver ions on different DNA templates were analyzed by using DFT calculations, and the conformational variations of DNA templates caused by silver ions and atoms were disclosed. Second, the aggregation behaviors of silver atoms constrained by the polymorphic DNA templates were studied by DFT modeling, and distinct fluorescence property of nanosilvers templated by polymorphic DNA were evaluated using the time-dependent DFT calculations. It is illustrated that with the DNA template adopting i-motif or the duplex the silver atoms tend to aggregate inside the encapsulated spaces of nucleobases, and the formed silver nanoclusters are positively charged with high fluorescent spectral features; whereas with the template of the G-quadruplex the silver atoms are preferential to aggregate outside of the G-tetrad, which results in the formation of larger silver crystals without fluorescence property. The results obtained here are useful to explore the nucleation and growth mechanism of silver nanomaterials regulated by the structure-specific DNA templates, which is important to rational design of desirable fluorescent emitters for sensing in the field from biology to nanoscience.



## 1. INTRODUCTION

DNA is a well-known biopolymer utilized to direct the synthesis of metal nanomaterials including Ag,<sup>1–5</sup> Au,<sup>6–8</sup> Ni,<sup>9</sup> Cu,<sup>10</sup> etc., owing to its unique recognition capabilities, and programmable self-assembly parameters.<sup>11</sup> Intriguingly, DNA-templated Ag nanomaterials have illustrated distinct physicochemical properties, involving the size, the fluorescence, and the catalytic activity, etc., dependent closely on DNA sequences or conformational structures.<sup>12–16</sup> For instances, Petty and co-workers produced red and green emissive silver clusters using the template of two i-motif forming oligonucleotides ( $dTA_2C_4)_4$  and  $(dC_4A_2)_3C_4$  with different loop sequences.<sup>4</sup> Zheng et al. reported that the size distribution and catalytic activity of Ag nanoparticles greatly depended on the polymorphic structure of DNA template, and the reduction reaction rate constants over these catalysts were in the decreasing order of i-motif-Ag > G-quadruplex-Ag > Duplex-Ag.<sup>17</sup> Additionally Fu et al. reported that double-stranded DNA templates can generate distinct fluorescent nanosilver modulated by the predominance among the structural competition of the Watson–Crick duplex, G-quadruplex, and i-motif.<sup>18</sup> Wang and co-workers reported that different Ag nanoclusters involving yellow to red emissive species templated by single-stranded oligonucleotide with several G-tracts and C-tracts on its two terminals can be regulated by adding K<sup>+</sup> and H<sup>+</sup>, which

enable the hairpin DNA to convert into the G-quadruplex or i-motif structures.<sup>19</sup> These results suggest that polymorphic DNA templates play an important role in adjusting the nucleation and growth of metal nanoparticles. Although previous experimental studies suggested that Ag<sup>+</sup> favors Lewis acid–base interactions with the electron-rich nitrogen and oxygen atoms of the nucleobases,<sup>20,21</sup> the mechanism of polymorphic DNA-template controlling on the growth and optical properties of silver clusters is not well understood, which is fundamental to develop DNA-directed controllable synthesis of nanoparticles with desirable physicochemical properties and promising applications in selective catalysis, sensitive sensing, and enhanced imaging.<sup>22–24</sup>

Dynamics simulations and quantum chemical calculations have been considered as a promising route to investigate the underlying mechanism on how biomolecular templates regulate the growth of metal nanomaterials. Behrens et al. used molecular dynamics simulations to calculate the interaction Pd nanoparticles and self-assembled protein templates to reveal the constrained growth process of catalytically active Pd nanoparticles.<sup>25</sup> Mpourmpakis et al. performed density func-

Received: July 2, 2011

Revised: January 10, 2012

Published: January 13, 2012



tional theory (DFT) calculations and molecular dynamics (MD) simulations to investigate the stability and growth of small ( $n = 1\text{--}12$ )  $\text{Au}_n(\text{SR})_n$  complexes with *p*-mercaptopbenzoic acid (MBA) as the thiolate capping agent SR.<sup>26</sup> However, as for the DNA–Ag complex system, molecular dynamics simulation on the interactive mechanism was obstructed from the lack of reliable force fields for the treatment of Ag, only some theoretical calculations based on simplified models were performed to study the inner interactions between the DNA nucleobases and  $\text{Ag}^+$  or  $\text{Ag}_n$ . Recently the ab initio density functional theory calculations were carried out to investigate the interaction of  $\text{Ag}^+$  with single adenine and cytosine base, the adenine-cytosine mispairs,<sup>27</sup> and the Watson–Crick guanine-cytosine base pairs,<sup>28</sup> to study the coupling of metal with DNA nucleobases. Meanwhile, Verdugo et al. constructed models of  $\text{Ag}_n$  ( $n = 1\text{--}6$ ) interacting with single base (A, C, G, and T) and showed that Ag-cluster isomers with distinct bases have different absorption spectra calculated by time-dependent DFT calculations.<sup>29</sup> So far no report has been found on investigating the nucleation and growth mechanism of silver clusters in the presence of DNA templates.

In this study, we performed the density functional theory calculations to study the aggregation behaviors of silver atoms modulated by polymorphic DNA templates involving i-motif, G-quadruplex, and the Watson–Crick duplex, combining with the experimental characterizations of CD, UV, fluorescence measurements, and TEM, to understand the reason in the molecular level that polymorphic DNA templates affect the fluorescence emitting species of Ag nanomaterials. First, the affinity sites of silver ions on different DNA templates were analyzed by using DFT calculations, and the conformational variations of DNA templates caused by silver ions and atoms were disclosed. Second, the aggregation behaviors of silver atoms constrained by the polymorphic DNA templates were studied by DFT modeling, and distinct fluorescence property of nanosilvers templated by polymorphic DNA were evaluated using the time-dependent DFT calculations. The results obtained here are useful to explore the nucleation and growth mechanism of silver nanomaterials regulated by the structure-specific DNA templates, which is important to rational design of desirable fluorescent emitters for sensing in the field from biology to nanoscience.

## 2. EXPERIMENTAL METHODS AND THEORETICAL CALCULATIONS

**2.1. Experimental Section.** Oligonucleotides d[G<sub>4</sub>T<sub>4</sub>G<sub>4</sub>] and d[C<sub>4</sub>A<sub>4</sub>C<sub>4</sub>], were purchased from the Japanese Takara Bio. (Dalian) with the purity higher than 98% measured by HPLC. All DNA samples were annealed by heating the sample cuvette to 95 °C for 5 min and then cooling to 4 °C. Silver nanomaterials were synthesized by adding  $\text{AgNO}_3$  to DNA samples incubated for 0.5 h at the molar ratio of  $[\text{Ag}^+]/[\text{DNA}]$  of 4, and then adding different amount of  $\text{NaBH}_4$  to reduce  $\text{Ag}^+$  for 8 h. To discuss clearly, Ag nanomaterials were named in terms of the DNA template, that is, Gq-Ag was denoted to Ag nanomaterials templated by the G-quadruplex, while Im-Ag and Du-Ag were templated by the i-motif and Watson–Crick duplex, respectively.

Circular dichroism (CD) experiments were carried out with a Jasco J-810 spectropolarimeter equipped with a Julabo temperature controller. Each sample was scanned from the wavelength of 220 to 350 nm at 20 °C. UV melting profiles were performed on a Cary 300 UV-vis spectrophotometer

equipped with a digital circulating water bath (Varian). The absorbance of G-rich sequences and double-stranded sequences was monitored at 295 and 260 nm, respectively, in a cuvette of 1 mm path length with a heating rate of 0.5 °C min<sup>-1</sup>. Fluorescence excitation and emission of silver nanomaterials were performed with a Cary Eclipse (Varian Ltd.) spectrofluorometer at 20 °C. Transmission electron microscopy was performed on JEM-2010FEF equipment (JEOL, Japan). TEM samples were prepared by applying 10  $\mu\text{L}$  samples on a carbon-coated grid for 5 min, followed by removing the excess liquid with the filter paper.

**2.2. Calculation Methods.** The first geometry optimization calculations were carried out using density functional theory (DFT) at the generalized gradient approximation (GGA) level of theory as implemented in the DMOL3 module of Materials Studio software supplied by Accelrys Inc. The PW91<sup>30,31</sup> exchange-correlation energy function was used throughout, together with the DNP basis set. This basis set includes a polarization p-function on all hydrogen atoms which can get best accuracy for hydrogen bonding. Because of the large amounts of molecules in DNA samples studied here, the convergence criteria were defined as follows: energy,  $E = 2.0 \times 10^{-5}$  hartree; gradient,  $\text{Grad} = 4 \times 10^{-3}$  hartree Å<sup>-1</sup>; Cartesian coordinates,  $\text{coord} = 5 \times 10^{-3}$  Å. A spin-restricted formalism was applied, considering the effect of the solvent,<sup>32,33</sup> and all the atoms were allowed to be relaxed during the geometry optimization process.

Then in the absorption spectra calculation, a rather large orthorhombic unit cell of size 15 × 15 × 15 Å<sup>3</sup> was built for the optimized structure of DNA–Ag complex. All the calculations in this study were carried out using density functional theory at the generalized gradient approximation (GGA) level of theory as implemented in the CASTEP module of Materials Studio software supplied by Accelrys Inc. The RPBE exchange-correlation energy functional and the Ultrasoft pseudopotentials were used here. The wave functions were represented by a plane wave basis set with a cutoff energy of 400.0 eV. The SCF tolerance was set as  $2.0 \times 10^{-6}$  eV atom<sup>-1</sup>, and a  $k$ -point separation 0.05 Å<sup>-1</sup> appropriate to the medium quality level was used for  $k$ -point grid. Calculations were made for three perpendicular light polarizations. The time-dependent Kohn–Sham (TD-KS) equations are used to propagate the state of the system for a finite time, and as to the metals, 2 eV plasma frequencies and 0.02 eV broadening were used to see the absorption properties.

The adsorption energy ( $E_{\text{ad}}$ ) was calculated to investigate the binding probability and stability between the active sites of the bases and adsorbed species like  $\text{Ag}^+$ ,  $\text{Ag}_n$  ( $n = 1\text{--}6$ ), which was defined as below

$$E_{\text{ad}} = -[E_{\text{complex}} - E_{\text{DNAsubstrate}} - E_{\text{guest}}]$$

where  $E_{\text{complex}}$  is the total energy of the DNA substrate binding with guest ions or molecules ( $\text{Ag}^+$  or  $\text{Ag}_n$ ) and  $E_{\text{DNAsubstrate}}$  and  $E_{\text{guest}}$  are the energy of the bare DNA substrate and the free guest species, respectively.

The beneficial binding sites of  $\text{Ag}^+$  or  $\text{Ag}_n$  onto DNA can be deduced through analyzing the adsorption energy. A positive value of  $E_{\text{ad}}$  indicates a preferential binding, and the larger the value the more stable the binding between the guest and the DNA.

## 2.3. Calculation Models of Polymorphic DNA Templates. 2.3.1. Models of Polymorphic DNA Templates.

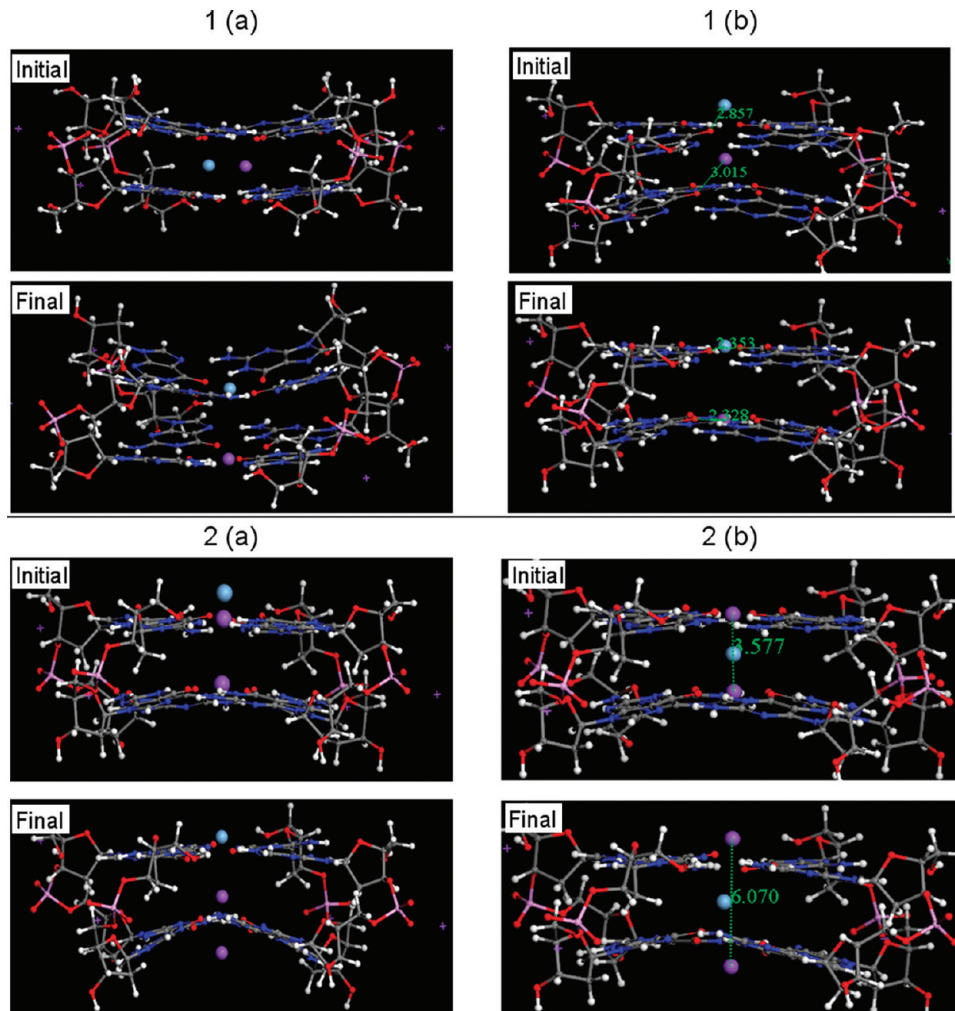


**Figure 1.** Competitive binding of one silver ion with the G-quadruplex model against prebound one sodium ion (1) or two sodium ions (2) with different initial positions (a and b): Na, purple; Ag, light blue; H, white; O, red; N, blue; P, pink; C, gray.

Three experimental structures are chosen as starting models, including the antiparallel G-quadruplex structure (PDB 1EVM) for the single-stranded d[G<sub>4</sub>T<sub>4</sub>G<sub>4</sub>], the i-motif structure (PDB 1CN0) for the single-stranded d[C<sub>4</sub>A<sub>4</sub>C<sub>4</sub>], and the standard duplex structure (PDB 3IXN) for the double-stranded d[G<sub>4</sub>T<sub>4</sub>G<sub>4</sub>]–[C<sub>4</sub>A<sub>4</sub>C<sub>4</sub>]. Because of the huge amounts of interactive molecules involved in the calculations, substantially calculating models were established through adopting appropriate fragments consisted of certain nucleotides from the above three original models, that is, the fragment of GG was used to represent the G-quadruplex template, CCCC to the i-motif, while the duplex has several fragment models of GG/CC, GGG/CCC, or GGGG/CCCC.

It is known that G-quartets stabilized by cyclic Hoogsteen hydrogen bondings are the building blocks of the G-quadruplexes,<sup>34–36</sup> and the monovalent ions such as Na<sup>+</sup> and K<sup>+</sup> play important roles in stabilizing the G-quadruplex.<sup>37–39</sup> Therefore we investigated the interaction between the monovalent ions (Na<sup>+</sup>, K<sup>+</sup>) and the fragment model of the G-quadruplex (GG), aiming to illustrate the feasibility of replacement of G-quadruplex by the fragment GG. In the presence of one single sodium ion, the simulation result indicates that in the final optimized structures the sodium ion locates preferentially in the middle between two neighboring G-tetrad planes no matter the sodium ion is initially placed in the

center of the G-tetrad plane or the middle between two G-tetrad planes (Figure S1-1 in the Supporting Information). It is consistent with previous experimental works suggesting the preferential location of sodium ions between the stacked quartets.<sup>40–44</sup> Moreover, the distances between the sodium ion and the O6 atoms of guanines are ranged from 2.823 to 2.799 Å in the final optimized structures, which agree well with 2.826 Å reported by other computational studies.<sup>44</sup> In the case of two sodium ions with one initial location in the middle between two G-planes and the other beyond the top G-plane, the final optimized structures indicate that two sodium ions locate closely to the two G-plane centers respectively in the fragment model GG (as shown in Supporting Information Figure S1–2a). Previously, there has been reported that the central Na<sup>+</sup> was easily driven away from its equilibrium position toward a G tetrad under the influence of the neighboring sodium ions.<sup>44</sup> Additionally for two potassium ions that have the radius of 1.33 Å, larger than that of sodium ions (0.95 Å), the final optimized structures indicate that one potassium ion locates in the distance of 2.99 Å away from the O6 atom of guanines and the other in the distance about 2.84 Å (Supporting Information Figure S1–2b). These distances are in accordance with the previous computational result of 2.95 Å for the location of one K<sup>+</sup> in two successive G-tetrads.<sup>44</sup> Thus it is reasonable to conclude that computational studies based on the fragment

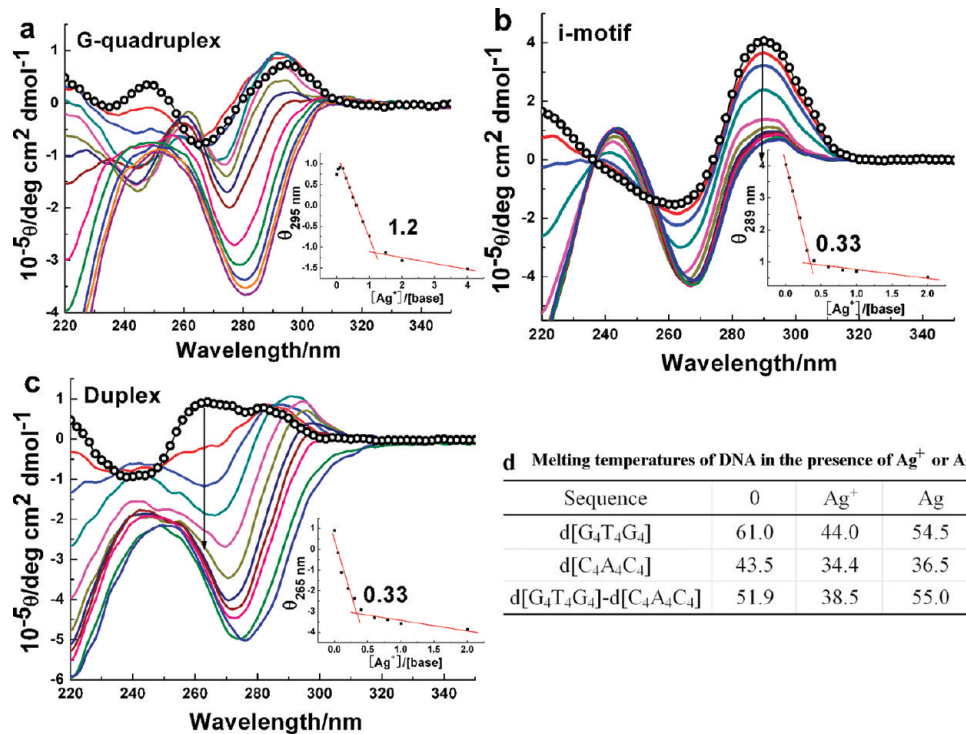


**Figure 2.** CD spectra of d[G<sub>4</sub>T<sub>4</sub>G<sub>4</sub>] at pH 7.0 (a), d[C<sub>4</sub>A<sub>4</sub>C<sub>4</sub>] at pH 5.0 (b), d[G<sub>4</sub>T<sub>4</sub>G<sub>4</sub>]-d[C<sub>4</sub>A<sub>4</sub>C<sub>4</sub>] at pH 7.0 (c) titrated with  $\text{Ag}^+$  ( $[\text{Ag}^+]/[\text{base}] = 0.05\text{--}4$ ), the black circle represent the spectrum of DNA alone, and the inset plots the intensity of the characteristic band of DNA with  $[\text{Ag}^+]/[\text{base}]$ ; (d) melting temperatures of DNA in the presence of  $\text{Ag}^+$  or Ag ( $[\text{Ag}^+]/[\text{base}] = 0.33$ ).

model GG can provide results accurate enough to disclose the characteristics of G-quadruplex DNA template.

**2.3.2. Competitive Binding of  $\text{Ag}^+$  with the G-Quadruplex against  $\text{Na}^+$ .** In the synthesis procedure of silver nanomaterials templated by the G-quadruplex DNA, the first step is to add  $\text{AgNO}_3$  aqueous solution into DNA buffer containing 83.3 mM  $\text{Na}^+$ , suggesting that the G-quadruplex DNA has been stabilized by the bound sodium ions before the addition of  $\text{AgNO}_3$ . Thus it is important to study whether or not the introduced silver ions can interact with the G-quadruplex against the prebound sodium ions.

It is known that  $\text{Ag}^+$  is favorable to interact with the electron-rich nitrogen and oxygen atoms of the nucleobases,<sup>20,21</sup> consequently one silver ion was placed initially in the neighborhood of nitrogen and oxygen atoms located in the center of the G-tetrad in the presence of prebound one (Figure 1, part 1) or two sodium ions (Figure 1, part 2). According to the computational optimization results, the silver ion is capable of expelling the prebound sodium ions from the original positions, and resulting in somewhat distortion of the G-quartet that can interact with both silver and sodium ions.

As far as the radius of silver ions (1.26 Å), a little larger than that of sodium ions (0.95 Å), is considered, the preferential binding site of one silver ion in the fragment model of GG was studied in the absence of sodium ions. It is suggested that the final optimized position of the silver ion is related to its initial location, with the Mulliken atomic charge ranged from 0.467 to 0.580 (Figure S2 in the Supporting Information). Comparing with the Mulliken atomic charge 0.807 of one sodium ion bound with the fragment model GG (Supporting Information Figure S1-1), it is easy to understand that electrostatic interactions between silver ions and the GG model are stronger than those between sodium ions and GG. The result confirms

that silver ions can competitively interact with O6 atoms of the G-quadruplex even if there exist prebound sodium ions in the G-quadruplex.

### 3. RESULTS AND DISCUSSION

**3.1. Fluorescent Silver Nanomaterials Regulated by Polymorphic DNA Templates.** The oligonucleotide d[G<sub>4</sub>T<sub>4</sub>G<sub>4</sub>], d[C<sub>4</sub>A<sub>4</sub>C<sub>4</sub>], and d[G<sub>4</sub>T<sub>4</sub>G<sub>4</sub>]-d[C<sub>4</sub>A<sub>4</sub>C<sub>4</sub>], with the initial conformational structure of G-quadruplex, i-motif, and the duplex, was adopted respectively as the DNA templates to synthesize silver nanomaterials. CD spectra of these DNA solutions show significant variations upon adding  $\text{Ag}^+$ . In the case of d[G<sub>4</sub>T<sub>4</sub>G<sub>4</sub>] template, the characteristic G-quadruplex CD band at 295 nm shows a blue-shift about 2 nm and a slight increase of the band intensity as the  $[\text{Ag}^+]/[\text{base}]$  molar ratio increases from 0.05 to 0.2 (Figure 2a). Whereas this positive peak gradually disappears, accompanying with the appearance of a negative band around 280 nm, as the  $[\text{Ag}^+]/[\text{base}]$  ratio increases continuously to 4.0. Through plotting the band intensity at 295 nm versus the  $[\text{Ag}^+]/[\text{base}]$  ratio, there exists a clear transition point at the  $[\text{Ag}^+]/[\text{base}]$  ratio of 1.2, which is corresponding to the binding stoichiometry of  $\text{Ag}^+$  to DNA base. Previously Loo et al. studied the interactions of silver ions and guanosine monophosphate by the calorimetry experiments, and reported that the empirical stoichiometry of  $\text{Ag}^+$ : nucleobase was about 1.<sup>45</sup> As the  $[\text{Ag}^+]/[\text{base}]$  ratio increases, the  $T_m$  value of d[G<sub>4</sub>T<sub>4</sub>G<sub>4</sub>] decreases greatly, e.g.,  $T_m$  of d[G<sub>4</sub>T<sub>4</sub>G<sub>4</sub>] decreases from the initial G-quadruplex of 61.0 to 56.4 °C and 55.2 and 41.0 °C at the  $[\text{Ag}^+]/[\text{base}]$  ratio of 0.08, 0.17, and 0.33 respectively (Figure 2d and Supporting Information Figure S3a), suggesting that addition of  $\text{Ag}^+$  destabilizes the G-quadruplex structure.

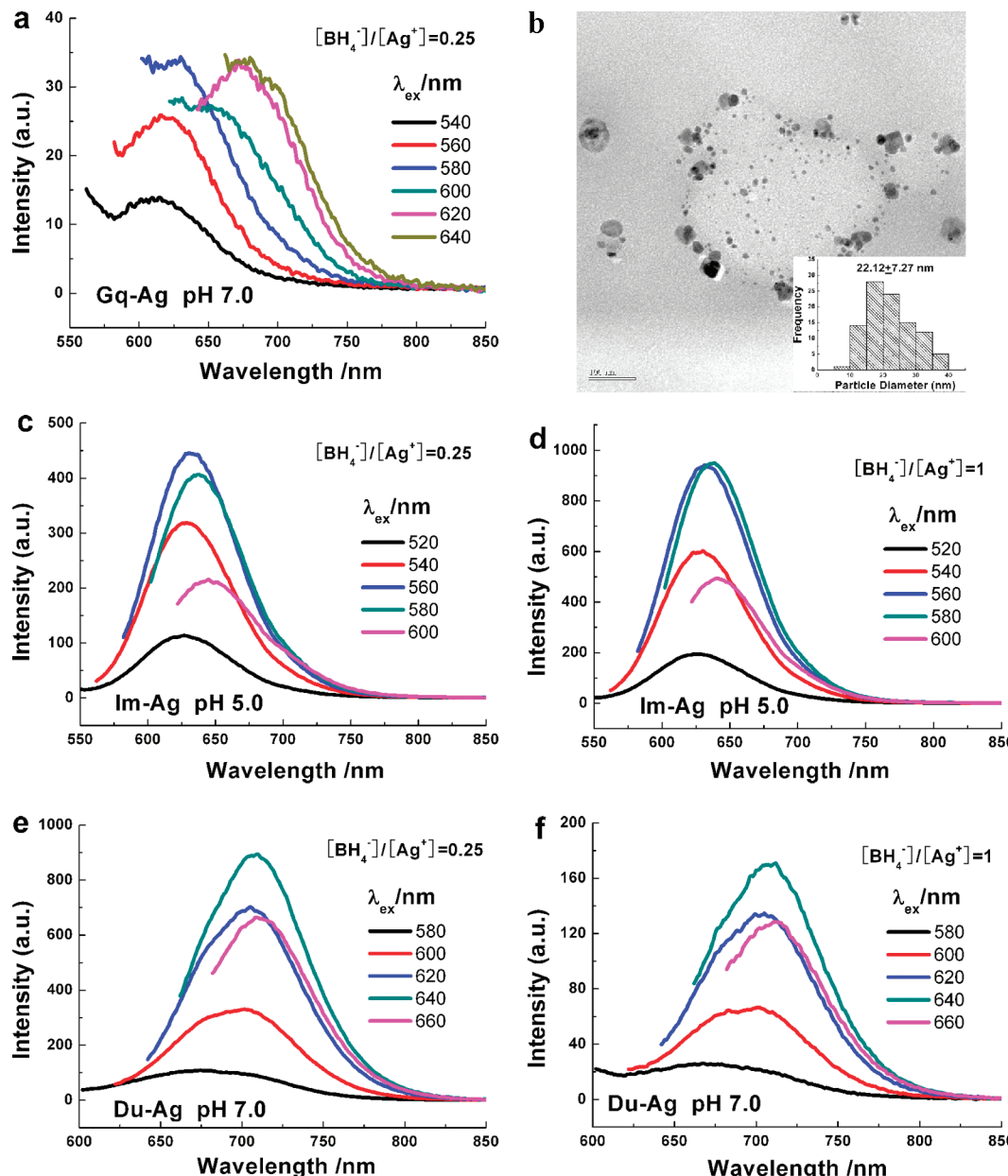


**Figure 3.** Fluorescence emission spectra of nano-Ag templated by the G-quadruplex  $d[G_4T_4G_4]$  at pH 7.0 with the  $[BH_4^-]/[Ag^+]$  ratio of 0.25 (a), the i-motif  $d[C_4A_4C_4]$  at pH 5.0 (c, d) and the duplex  $d[G_4T_4G_4]-d[C_4A_4C_4]$  at pH 7.0 (e, f) with  $[BH_4^-]/[Ag^+] = 0.25$  and 1.0 respectively; (b) TEM images of Ag templated by  $d[G_4T_4G_4]$  at  $[BH_4^-]/[Ag^+] = 1$ .

In the case of  $d[C_4A_4C_4]$  template, CD spectra indicate that the typical i-motif band at 289 nm decreases upon titration of  $Ag^+$ , and the plot of the band intensity versus the  $[Ag^+]/[base]$  ratio suggests the binding stoichiometry of  $Ag^+$  to nucleobase is about 0.33 (Figure 2b), which is almost one-third of that with  $d[G_4T_4G_4]$ . Such lower affinity of  $Ag^+$  is probably due to the distinct structural constraints in the i-motif structure, unlike that of the G-quadruplex. And the  $T_m$  value decreases from 43.5 °C of the pure i-motif to 34.4 °C with the  $[Ag^+]/[base]$  ratio of 0.33 (Figure 2d).

As for the template of  $d[G_4T_4G_4]-d[C_4A_4C_4]$ , CD spectra show that the typical duplex band at 265 nm has a distinct redshift to 290 nm as the  $[Ag^+]/[base]$  ratio increases from 0.05 to 0.2. And the intensity of the band at 290 nm decreases gradually and a negative peak near 275 nm is enhanced as increasing  $[Ag^+]/[base]$  ratio. The binding stoichiometry of

$Ag^+$  to the duplex DNA is also about 0.33 (Figure 2c). The  $T_m$  value of  $d[G_4T_4G_4]-d[C_4A_4C_4]$  decreases from the pure duplex of 51.5 to 38.5 °C with the  $[Ag^+]/[base]$  ratio of 0.33 (Figure 2d).

It is worthwhile to note that the melting temperatures of DNA solutions are increased upon reduction  $Ag^+$  into Ag by adding  $NaBH_4$ . Figure 2d displays that the  $T_m$  value of  $d[G_4T_4G_4]$ ,  $d[C_4A_4C_4]$ , and  $d[G_4T_4G_4]-d[C_4A_4C_4]$  in the presence of Ag is 54.5, 36.5, and 55.0 °C, respectively, much higher than that in the presence of  $Ag^+$  with the  $[Ag^+]/[base]$  ratio of 0.33. In addition, CD spectra of  $d[G_4T_4G_4]$ ,  $d[C_4A_4C_4]$ , and  $d[G_4T_4G_4]-d[C_4A_4C_4]$  at the same conditions exhibit their characteristic band at 295, 289, and 287 nm, respectively (Supporting Information Figure S3b), suggesting that each of the DNA templates still maintains distinct individual structural characteristics.

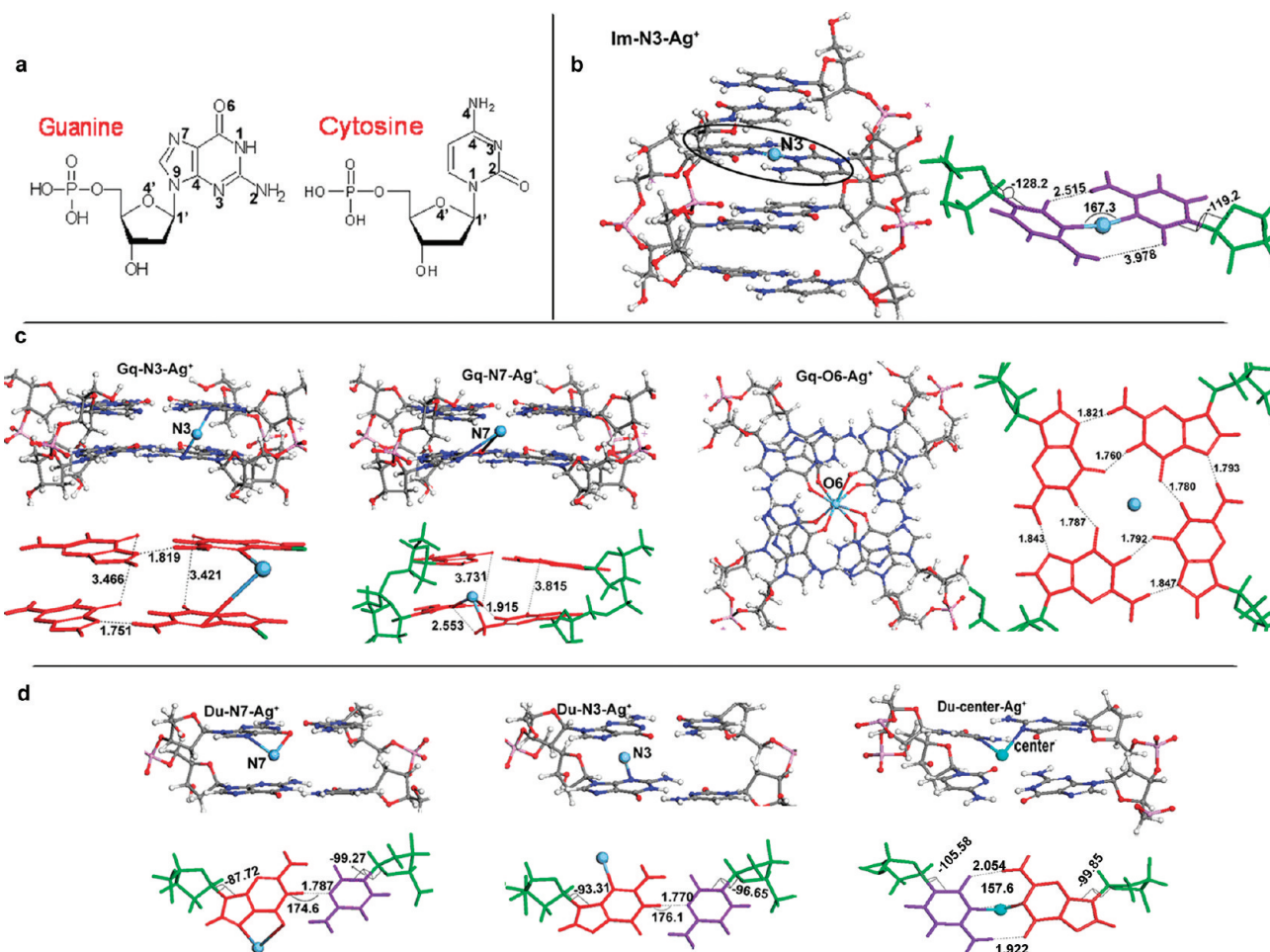


**Figure 4.** Numbered atomic sites in the G or C base (a), and affinity sites of one silver ion on DNA templates with the structure of i-motif (b), G-quadruplex (c), and the duplex (d), respectively. In the stick model, Ag = light blue, cytosine = purple, guanine = red, phosphate backbone = green.

Nanosilvers templated by polymorphic DNA templates involving the G-quadruplex, the i-motif and the duplex show distinct fluorescent properties associated with the molar ratio of  $[BH_4^-]/[Ag^+]$ . As shown in Figure 3a, the emission spectra of Ag nanomaterials templated by the G-quadruplex d[G<sub>4</sub>T<sub>4</sub>G<sub>4</sub>] (Gq-Ag) shift with the excitation wavelengths and exhibit the strongest emission at 628 and 672 nm as the  $[BH_4^-]/[Ag^+]$  ratio is 0.25, suggesting the complex formation between small silver clusters and d[G<sub>4</sub>T<sub>4</sub>G<sub>4</sub>] with varying stoichiometric ratios.<sup>1</sup> Whereas no fluorescence is detectable for Gq-Ag synthesized at the  $[BH_4^-]/[Ag^+]$  ratio of 1.0, of which the average size of obtained silver nanoparticles is about 22.12 nm (Figure 3b).

Intriguingly, nanosilvers templated by the i-motif d[C<sub>4</sub>A<sub>4</sub>C<sub>4</sub>] display the red emission at 638 nm under the  $[BH_4^-]/[Ag^+]$  ratio of 0.25 (Figure 3c), and the fluorescence intensity at 638 nm is enhanced about twice as the  $[BH_4^-]/[Ag^+]$  ratio increases to 1.0 (Figure 3d). As for the nanosilvers template by the duplex d[G<sub>4</sub>T<sub>4</sub>G<sub>4</sub>]-d[C<sub>4</sub>A<sub>4</sub>C<sub>4</sub>], the prominent near-IR emitters are detected at 708 nm under the  $[BH_4^-]/[Ag^+]$  ratio of 0.25 (Figure 3e), while the fluorescence intensity is decreased by about 80% as the  $[BH_4^-]/[Ag^+]$  ratio increases to 1.0 (Figure 3f).

Previously, Koszinowski et al. reported that a highly charged fluorescent Ag<sub>6</sub><sup>4+</sup> cluster can be synthesized with the template of oligonucleotide dC<sub>12</sub> at basic or neutral conditions.<sup>46</sup> Guo et al. reported that yellow fluorescent emitters stabilized by a

duplex structure were probably due to partly reduced Ag clusters.<sup>47</sup> Therefore, the changes of fluorescence emission are attributed to distinct charge states of DNA-templated Ag associated with the stoichiometric ratio of the reduction agent. In addition, our previous work<sup>18</sup> reported that Im-Ag and Du-Ag have an average size of 3.64 and 1.59 nm respectively at the  $[BH_4^-]/[Ag^+]$  ratio of 1.0, and consequently it is suggested that Ag templated by the G-quadruplex are liable to grow into larger crystals with no fluorescence property, compared with those templated by the i-motif and the duplex.

To understand the reason in the molecular level that polymorphic DNA templates affect the emitting species of Ag nanomaterials, we further performed the density functional theory calculations to analyze the difference of the nucleation and growth of Ag clusters along DNA templates. In the following context, DFT calculations are first performed to understand the optimized binding modes of silver ions to different DNA templates to give deep insights to the variations of CD spectra and thermodynamic data mentioned in section 3.1. Second, the preferential nucleation sites of silver atoms on the polymorphic DNA templates are calculated by DFT modeling to study aggregation behaviors of silver atoms constrained by the templates, as well as to illustrate distinct fluorescence property of nanosilvers templated by polymorphic DNA.

### 3.2. Affinity Sites of Ag(I) and Ag(0) on Polymorphic DNA Templates.

It is fundamental to discriminate potential

affinity sites of DNA templates with silver ions and atoms, so as to disclose the influence of DNA templates on the nucleation and growth of nanosilver. Previous work suggested that the interactive sites of  $\text{Ag}^+$  are mainly the electron-rich nitrogen and oxygen atoms of the nucleobases, such as the N3, N1, and N7 atoms of adenine (A), the N7, N3, the deprotonated N1 and O6 of guanine (G), the N3 of cytosine (C)<sup>21,48</sup> and the deprotonated N3 of thymine (T).<sup>3</sup> Accordingly, we constructed the initial calculation models involving one silver ion and different DNA templates. The optimized results illuminate potential affinity sites of Ag(I) on DNA templates involving the i-motif, the G-quadruplex and the duplex, as displayed in Figure 4.

In the case of the i-motif template, there exists only one N3 site of cytosine to interact with Ag(I) (Figure 4b), and the optimized results indicate that the C–Ag–C pairing is formed through the interaction of N3–Ag, and the distance between N3 and Ag(I) is 2.134 Å. The formation of C–Ag–C pairing results in a change of the linearity of the bond and planarity between two cytosines, that is, the linear (N3–Ag–N3) and dihedral ( $\text{C}_4\text{--N}_3\text{--N}_3\text{--C}_4$ ) angles decrease from the initial 176.5° and –168.1° to 167.3° and –164.3°, respectively. Additionally the torsion angles between the base and its attached sugar radical for O4’–C1’–N1–C2 in cytosine change by from the initial –129.4° and –119.9° to –128.2° and –119.2°, respectively. As the number of silver ions increases to four, further calculations on interactions of four silver ions with the i-motif suggest that N3 sites are the only affinity sites toward Ag(I) (Supporting Information Figure S4), and the largest distance between two cytosine is increased by 51.42%. It is illustrated that the formation of C–Ag–C cannot destroy the i-motif structure of DNA template other than change the linearity of the bond and planarity between two cytosines, which is in accord with the small decrease of melting temperature of  $d[\text{C}_4\text{A}_4\text{C}_4]$  in the presence of silver ions (Figure 2).

For the G-quadruplex template, there are three kinds of affinity sites of Ag(I), that is, the center of eight O6 atoms in the neighborhood G-tetrads, N7 and N3 sites (Figure 4c). According to the optimized results, the adsorption of Ag(I) at the center of eight O6 atoms makes the distance between two G-tetrad planes increased from 3.375 to 3.434 Å, and the similar distance increase between two G-planes is observed in the N3–Ag complex, while in the N7–Ag complex, the hydrogen bond N2–H2…N7 is weakened owing to the distance enlarged from 1.718 to 2.553 Å besides the enlarged distance 3.731 and 3.815 Å of two G-tetrad planes. These enlarged distances between two G-planes and the poor base packing between neighboring guanines result in the decrease of  $T_m$  value of the G-quadruplex system in the presence of silver ions (Figure 2).

For the duplex template, there are also three kinds of affinity sites of Ag(I), that is, N7, N3, and the center of G–C pair (Figure 4d). According to the optimized results, the adsorption of Ag(I) at N7 site makes the included and the dihedral angles between guanine and cytosine decreased from the initial 176.3° and 176.3° to 174.6° and 174.5°, and the torsion angle that is related with G and C changed respectively from the initial –94.05° and –97.21° to –87.72° and –99.27°. In the Figure 4d, there also list the changed conformational parameters for the duplex DNA caused by the interaction of Ag(I) with N3 and the center of G–C pair, respectively. It is noteworthy that the variations of included, dihedral and torsion angles caused by

Ag(I) make the base packing weakened significantly, which results in the obvious decrease of  $T_m$  value of the duplex system in the presence of silver ions (Figure 2).

Moreover, CD spectra and thermodynamic data shown in Figure 2 indicate that the melting temperatures of DNA solutions are increased upon reduction  $\text{Ag}^+$  into Ag, which enlighten us to compare the adsorption energy  $E_{ad}$  of Ag(I) with that of Ag(0). Table 1 lists  $E_{ad}$  values of Ag(I) and Ag(0)

**Table 1. Adsorption Energies of Ag(I) and Ag(0) to Polymorphic DNA Templates**

affinity sites	$E_{ad}$ (eV)	
	Ag(I)	Ag(0)
Im-N3	2.03	2.44
Gq-O6	2.34	3.4
Gq-N3	0.76	1.97
Gq-N7	0.98	2.22
Du-N7	1.45	2.83
Du-N3	1.09	2.52
Du-center	2.03	3.04

on the affinity sites of different DNA templates determined through the above optimization results. The more positive value of  $E_{ad}$ , the more preferential binding toward the guest molecule (Ag(I) or Ag(0)). On the site of N3 in cytosine of the i-motif template (Im–N3), the  $E_{ad}$  value of Ag(0) is a little larger than that of Ag(I). While on the sites of O6, N3, N7 in guanine of the G-quadruplex, the  $E_{ad}$  values of Ag(0) are much higher than those of Ag(I), and so do the  $E_{ad}$  values of Ag(I) and Ag(0) on the sites of N3, N7 in guanine and the center of G–C base pair of the duplex. Comparing the variations of included, dihedral and torsion angles caused by Ag(0) with those by Ag(I), it is illustrated that the overlapped areas between axially neighboring bases are partially restored so that the base packings of DNA in the presence of Ag(0) are superior to those in Ag(I). Therefore, it is the restored base packings caused by reduction of  $\text{Ag}^+$  that result in the much higher increases of  $T_m$  values for the G-quadruplex and the duplex.

**3.3. Aggregation Behaviors of Silver Atoms Modulated by Polymorphic DNA Templates.** To disclose the effect of DNA templates on the nucleation and growth of silver nanoclusters, we studied the aggregation of silver atoms bound initially at the affinity sites discussed in the section 3.2, as well as that with bound silver atoms and other free silver atoms around since unbound silver ions usually exist in the experiment.

Adopting i-motif DNA as the template, the geometric optimization results indicate that the silver atoms bound initially at the affinity sites aggregate to form two double-atom nanoclusters encapsulated by two tilted tandem C–C pairs, with the distance between two silver atoms is about 2.633 Å (the left panel in Figure 5a). These two nanoclusters interact with surrounding DNA bases through Ag–N bondings except for physical adsorptions, and the corresponding  $E_{ad}$  values suggest strong bindings of these nanoclusters with DNA template, as shown in the top panel of Figure 5b. When there exist free silver atoms surrounded the i-motif, the optimized results indicate the formation of several Ag nanoclusters including 2–4 silver atoms, with the Ag–Ag distance about 2.728 Å. There are substantial interactions between the surrounded nucleobases and the silver nanoclusters through Ag–N bondings (the right panel in Figure 5a and the bottom

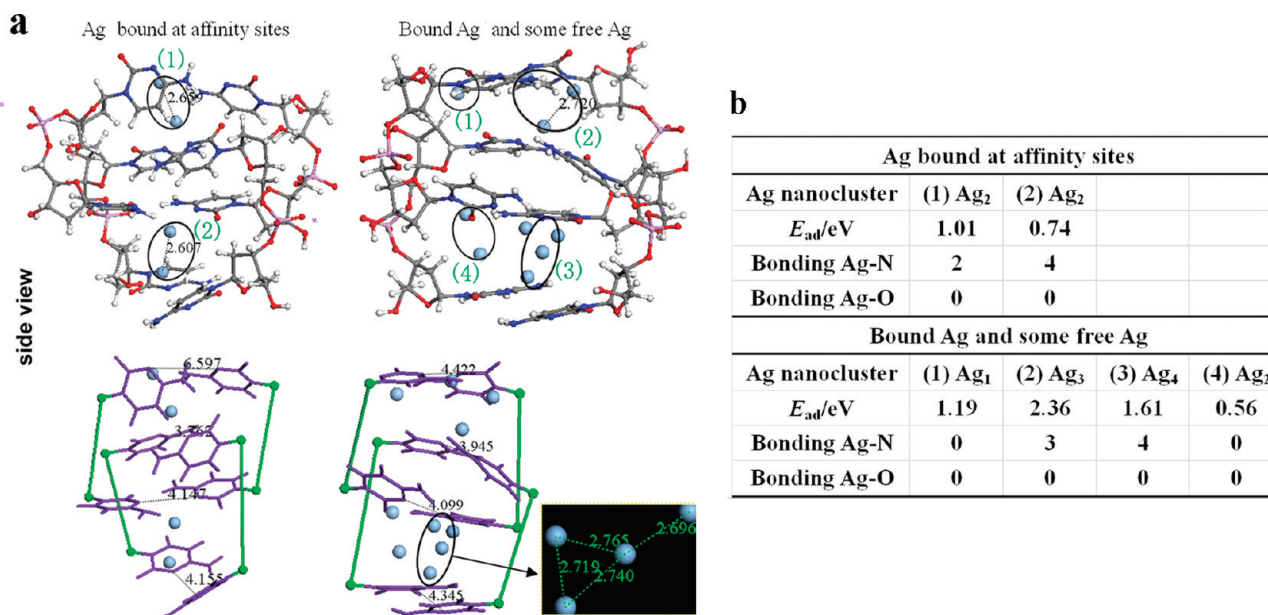


**Figure 5.** (a) Aggregation behavior of Ag atoms templated by i-motif, together with the display using the simple stick model: Ag, light blue; cytosine, purple; phosphate backbone, green. (b) Adsorption energies and silver–DNA ligations of different Ag nanoclusters with surrounding DNA nucleobases.

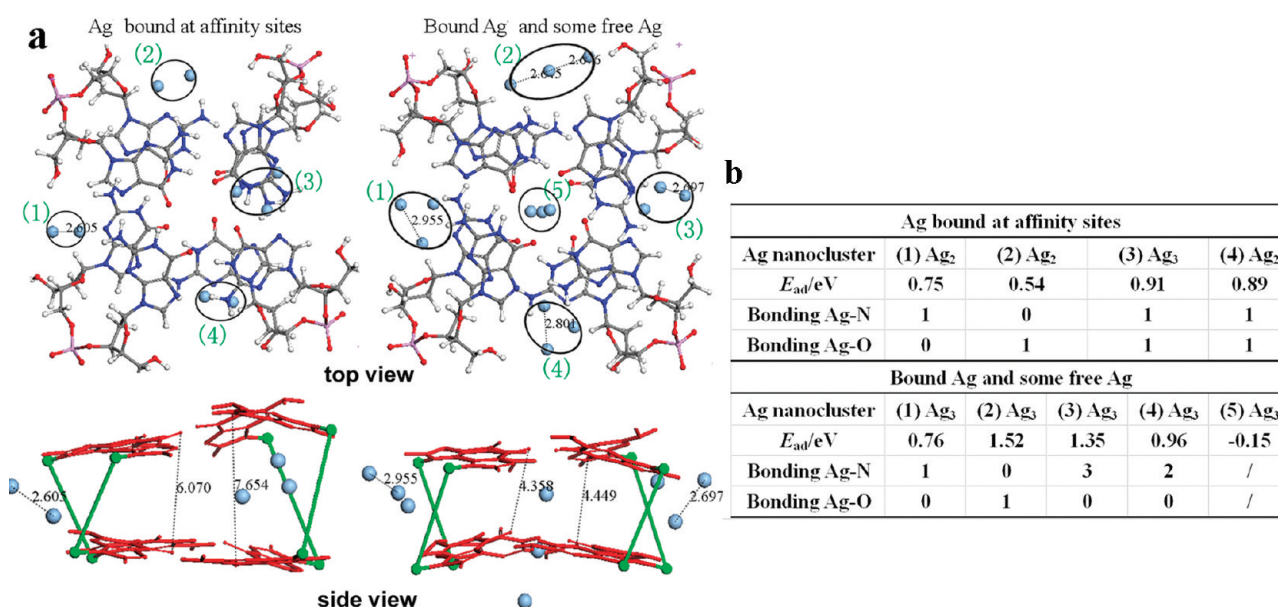


**Figure 6.** (a) Aggregation behavior of Ag atoms templated by the G-quadruplex, together with the display using the simple stick model to show the plane–plane distance in the side view: Ag, light blue; guanine, red; phosphate backbone, green. (b) Adsorption energies and silver–DNA ligations of different Ag nanoclusters with surrounding DNA nucleobases.

of Figure 5b), and the discrepancy of preferential binding of the silver nanoclusters become larger. Through the simple stick i-motif model, it is clear that the DNA template maintains the typical structure of the i-motif even if there appear these silver nanoclusters inside the DNA scaffold.

As a control, the equilibrium distance between two individual Ag atoms in the absence of DNA template was calculated to be 2.599 Å (Supporting Information Figure S5). The above optimized Ag nanoclusters in the presence of DNA templates show a little longer distance between Ag atoms, reflecting the fact that the DNA templates do play an important role in regulating the aggregation of silver atoms.

As for the G-quadruplex template bound Ag atoms initially in the position of N7, N3, and the central site of eight O6 atoms, the optimized structures show that Ag atoms prefer to aggregate into silver nanoclusters, involving Ag<sub>2</sub> (1), Ag<sub>2</sub> (2), Ag<sub>3</sub> (3), and Ag<sub>2</sub> (4), outside of the G-tetrad (Figure 6a), the distances between the silver atoms and the binding site of N7 or N3 are enlarged from  $2.33 \pm 0.06$  to  $4.48 \pm 0.20$  Å, and the silver atom located in the center move away to join the aggregation outside of the G-tetrad. These silver nanoclusters, interacted with the G-quadruplex template through Ag–N or Ag–O bondings, make the guanine bases tilted and the distance between the two adjacent G-tetrads enlarged almost twice, as shown by the side view of the stick model in Figure 6a.  $E_{ad}$

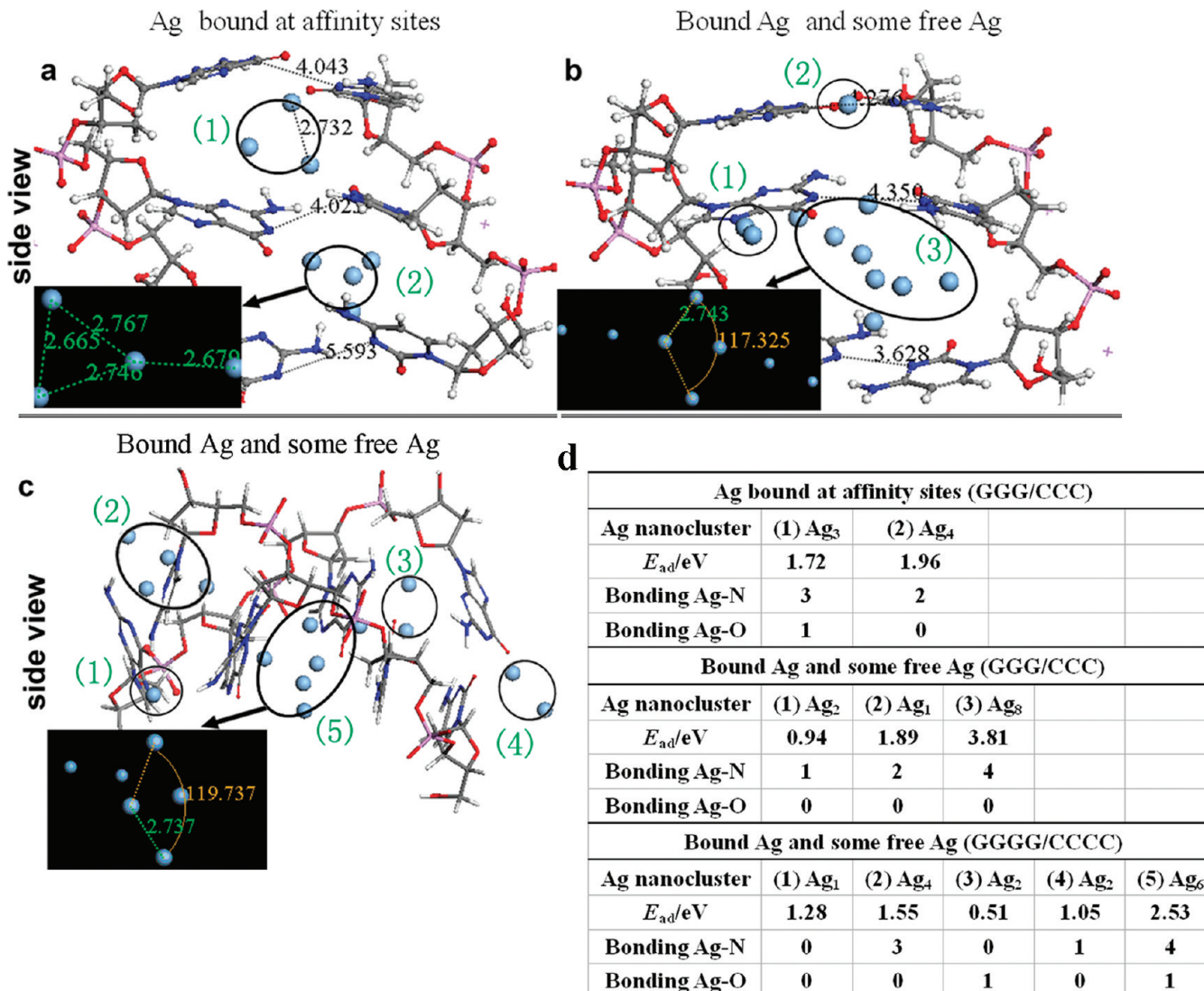


**Figure 7.** Aggregation behavior of bound Ag atoms (a) and bound and free Ag atoms (b) in the duplex (GGG/CCC) and (c) the aggregation behavior of bound and free Ag atoms templated by the larger duplex stick model GGGG/CCCC: Ag, light blue; H, white; O, red; N, blue; P, pink; C, gray. (d) Adsorption energies and silver–DNA ligations of different Ag nanoclusters with surrounding DNA nucleobases.

values of these silver nanoclusters suggest a little difference of preferential binding of the silver nanoclusters with the G-quadruplex (Figure 6b). When free silver atoms appear surrounding the G-quadruplex, after optimization four silver nanoclusters including three silver atoms are formed outside of the G-quartet, with positive  $E_{ad}$  values suggesting strong interactions with the nucleobases. The negative  $E_{ad}$  value of the silver atoms in the center of the G-quadruplex indicates an unstable intermediate state of those atoms, which are easy to move away to participate the aggregation surrounded the G-quartet.

For the duplex GGG/CCC template with Ag atoms bound at the affinity sites in both G and C bases, the aggregation of silver atoms makes the distances between the pairing G-C bases in two strands enlarged from 2.90 Å to 4.03 Å even 5.59 Å, and the dihedral angle between the G and C bases decreased by 7.941° even 64.65° after the optimization calculations (Figure 7a), similar optimization calculations were obtained for the fragment model of the duplex GG/CC template (Supporting Information Figure S6). The nanoclusters interact with surrounding nucleobases through Ag–N bondings and Ag–O

bonding (Figure 7d). When other free Ag atoms present around the duplex, the optimization calculations (Figure 7b) indicate the formation of a large nanocluster including eight Ag atoms, with the Ag–Ag distance of 2.76 ± 0.15 Å. Surrounded this eight-silver nanocluster, the distance between the pairing G-C bases in the complementary strands is about 4 Å, the dihedral angles of G and C base are partially restored, and there exist four Ag–N bondings between Ag<sub>8</sub> and DNA bases.

As far as the validity of the established fragment models of d[G<sub>4</sub>T<sub>4</sub>G<sub>4</sub>]-d[C<sub>4</sub>A<sub>4</sub>C<sub>4</sub>] template is considered, a larger fragment model GGGG/CCCC of the duplex was utilized to perform the geometry optimization of silver aggregation behaviors. As shown by Figure 7c, the largest silver nanocluster Ag<sub>6</sub> contains six silver atoms with the Ag–Ag distance of 2.83 ± 0.15 Å, approximate to the lattice spacing of 2.88 Å in the plane (111) of Ag nanocrystal (Supporting Information Figure S7). The nanocluster Ag<sub>6</sub> interacts with DNA bases through four Ag–N and one Ag–O bondings, meanwhile there are three other silver nanoclusters, that is, Ag<sub>4</sub>(2), Ag<sub>2</sub>(3), and Ag<sub>2</sub>(4), located separately along the double helix. Comparing with the optimization results based on the duplex fragment model of

GGG/CCC, it is illuminated that both models of GGG/CCC and GGGG/CCCC can reflect the fact that the nucleobases in the duplex DNA template do have a constraint effect on the aggregation of silver atoms.

Neidig et al. studied the DNA-templated silver nanoclusters by Ag K-edge EXAFS analysis, and reported that different DNA sequences lead to differences in silver-DNA ligation (Ag–N/O), as well as silver nanocluster size. They concluded that cooperative effects of Ag–DNA ligation and variations in cluster size lead to the tuning of the fluorescence emission of DNA templated silver nanoclusters.<sup>49</sup> The molecular modeling results obtained here, the first time, make it understandable how the polymorphic DNA template influence the size of silver nanoclusters and their interactions with nucleobases.

**3.4. Influences of Polymorphic DNA Structures on the Physical–Chemical Properties of Silver Clusters: Comparisons between Experimental Results and DFT Studies.** In the above section, DFT studies on the affinities of Ag(I) and Ag(0) with polymorphic DNA templates not only disclose the conformational variations of DNA templates caused by silver ions and atoms, which makes it clear to understand why the experimental  $T_m$  values of DNA are decreased by adding Ag<sup>+</sup> but restored by Ag atoms but also show the preferential binding sites of silver ions on nucleobases, that is, N3 in cytosine of the i-motif, the center of eight O6 atoms and N3, N7 in guanine of the G-quadruplex, the center of G–C base pairing and N7, N3 in guanine of the duplex. On the basis of these affinity sites, it is possible to evaluate the effect of polymorphic DNA templates on the formation of silver nanoclusters, enlightening us with the nucleation mechanism of silver nanocrystals modulated by polymorphic DNA templates. It is illustrated that with the DNA template adopting i-motif or the duplex the silver atoms tend to aggregate inside the encapsulated spaces of nucleobases, and the formed silver nanoclusters have strong interactions with DNA templates through Ag–N or Ag–O bondings; whereas with the template of the G-quadruplex the silver atoms are preferential to aggregate outside of the G-tetrad, which results in the formation of larger silver crystals without fluorescence property (see the experimental results in Figure 3).

To explore the reason that distinct fluorescence emission properties are detected for nanosilvers templated by polymorphic DNA, we chose typical three-atom silver nanoclusters of Im-Ag<sub>3</sub>, Gq-Ag<sub>3</sub>, and six-atom nanocluster of Du-Ag<sub>6</sub>, which are formed under the modulation of the i-motif, the G-quadruplex and the duplex, respectively, to carry out time-dependent DFT calculations to obtain their absorption spectra.<sup>29,50</sup> As shown in Figure 8, the adsorption energy ( $E_{ad}$ ) for the silver nanoclusters of Du-Ag<sub>6</sub> and Im-Ag<sub>3</sub> is 5.43 and 2.00 eV, respectively, much higher than that of Gq-Ag<sub>3</sub> (0.924 eV). And the nanoclusters of Du-Ag<sub>6</sub> and Im-Ag<sub>3</sub> are charged with +0.705 and +0.285 electrons respectively, while Gq-Ag<sub>3</sub> is negatively charged (-0.246 electrons). Previous studies reported that silver clusters synthesized on different DNA strands containing from a few to roughly ten silver atoms show distinct fluorescent species with excitation wavelengths of roughly 1.7–3.0 eV.<sup>12,13</sup> The absorption spectra in Figure 8 suggest that the excitation wavelength of Du-Ag<sub>6</sub> (2.40 eV) exhibits lower energy than Im-Ag<sub>3</sub> (2.82 eV) and Gq-Ag<sub>3</sub> (2.89 eV), which is consistent with the experimental results in Figure 3 that indicate the fluorescence emission species of nanosilvers locating at 638 nm templated by the i-motif, 672 nm templated by the G-quadruplex, and 708 nm templated by the duplex.

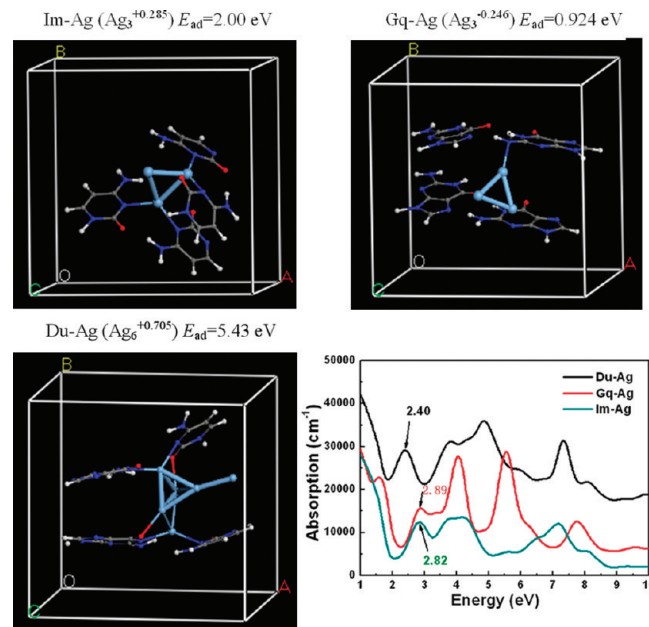


Figure 8. Absorption spectra of Du-Ag (the dark one), Gq-Ag (the red one), and Im-Ag (the green one).

However, the experimental results show that the fluorescence emission intensities of nanosilvers templated by the i-motif and the duplex are much stronger than those templated by the G-quadruplex. It is probably attributed to the difference of nanosilver's charges, i.e., the positively charged Ag nanoclusters templated by the duplex and i-motif are superior to possess high fluorescent spectral features, other than the negatively charged nanoclusters templated by the G-quadruplex.

#### 4. CONCLUSIONS

We performed the density functional theory calculations to study the aggregation behaviors of silver atoms modulated by polymorphic DNA templates involving i-motif, G-quadruplex, and the Watson–Crick duplex, combining with the experimental characterizations of CD, UV, fluorescence measurements, and TEM, to understand the reason in the molecular level that polymorphic DNA templates affect the fluorescence emitting species of Ag nanomaterials. First, through DFT calculations the affinity sites of silver ions on different DNA templates were analyzed, and the conformational variations of DNA templates caused by silver ions and atoms were disclosed, which makes it clear to understand the changes of CD spectra and thermodynamic data in the presence of silver ions and atoms. Second, the aggregation behaviors of silver atoms constrained by the polymorphic DNA templates were studied by DFT modeling, and distinct fluorescence property of nanosilvers templated by polymorphic DNA were evaluated using the time-dependent DFT calculations. It is illustrated that with the DNA template adopting i-motif or the duplex the silver atoms tend to aggregate inside the encapsulated spaces of nucleobases, and the formed silver nanoclusters are positively charged with high fluorescent spectral features; whereas with the template of the G-quadruplex the silver atoms are preferential to aggregate outside of the G-tetrad, which results in the formation of larger silver crystals without fluorescence property. The results obtained here are useful to explore the nucleation and growth mechanism of silver nanomaterials regulated by the structure-specific DNA templates.

## ■ ASSOCIATED CONTENT

### Supporting Information

Preferential location of one sodium ion, two sodium or potassium ions, and one silver ion in the fragment model of the G-quadruplex, interactions of four silver ions with the i-motif, the aggregation of bound Ag atoms templated by the duplex (GG/CC), the plane (111) of Ag nanocrystal, and the aggregation of two free Ag atoms. This material is available free of charge via the Internet at <http://pubs.acs.org>.

## ■ AUTHOR INFORMATION

### Corresponding Author

\*Address: Dr. Wei Li, Professor of Biochemical Engineering, School of Chemical Engineering and Technology, Tianjin University, Tianjin 300072, P.R. China. Tel: +86-22-27890643. Fax: +86-22-27890643. E-mail: liwei@tju.edu.cn.

### Notes

The authors declare no competing financial interest.

## ■ ACKNOWLEDGMENTS

We greatly appreciate Professor Dr. Charles Laughton, School of Pharmacy, University of Nottingham, U.K., for his useful suggestions on this article. This work was supported by NSFC (20836005, 21076141), the Special Funds for Major State Basic Research Program of China (2012CB720300), and the RFDP.

## ■ REFERENCES

- (1) Petty, J. T.; Zheng, J.; Hud, N. V.; Dickson, R. M. *J. Am. Chem. Soc.* **2004**, *126*, 5207–5212.
- (2) Ritchie, C. M.; Johnsen, K. R.; Kiser, J. R.; Antoku, Y.; Dickson, R. M.; Petty, J. T. *J. Phys. Chem. C* **2007**, *111*, 175–181.
- (3) Sengupta, B.; Ritchie, C. M.; Buckman, J. G.; Johnsen, K. R.; Goodwin, P. M.; Petty, J. T. *J. Phys. Chem. C* **2008**, *112*, 18776–18782.
- (4) Sengupta, B.; Springer, K.; Buckman, J. G.; Story, S. P.; Abe, O. H.; Hasan, Z. W.; Prudowsky, Z. D.; Rudisill, S. E.; Degtyareva, N. N.; Petty, J. T. *J. Phys. Chem. C* **2009**, *113*, 19518–19524.
- (5) Diez, I.; Ras, R. H. A. *Nanoscale* **2011**, *3*, 1963–1970.
- (6) Wang, Z. D.; Zhang, J. Q.; Ekman, J. M.; Kenis, P. J. A.; Lu, Y. *Nano Lett.* **2010**, *10*, 1886–1891.
- (7) Lalander, C. H.; Zheng, Y. H.; Dhuey, S.; Cabrini, S.; Bach, U. *ACS Nano* **2010**, *4*, 6153–6161.
- (8) Sharma, J.; Chhabra, R.; Andersen, C. S.; Gothelf, K. V.; Yan, H.; Liu, Y. *J. Am. Chem. Soc.* **2008**, *130*, 7820–7821.
- (9) Berti, L.; Alessandrini, A.; Menozzi, C.; Facci, P. *J. Nanosci. Nanotechnol.* **2006**, *6*, 2382–2385.
- (10) Su, Y. T.; Lan, G. Y.; Chen, W. Y.; Chang, H. T. *Anal. Chem.* **2010**, *82*, 8566–8572.
- (11) Egli, M.; Pallan, P. S. *Curr. Opin. Struct. Biol.* **2010**, *20*, 262–275.
- (12) Richards, C. I.; Choi, S.; Hsiang, J. C.; Antoku, Y.; Vosch, T.; Bongiorno, A.; Tzeng, Y. L.; Dickson, R. M. *J. Am. Chem. Soc.* **2008**, *130*, 5038–5039.
- (13) O'Neill, P. R.; Velazquez, L. R.; Dunn, D. G.; Gwinn, E. G.; Fygenson, D. K. *J. Phys. Chem. C* **2009**, *113*, 4229–4233.
- (14) Gwinn, E. G.; O'Neill, P.; Guerrero, A. J.; Bouwmeester, D.; Fygenson, D. K. *Adv. Mater.* **2008**, *20*, 279–283.
- (15) Driehorst, T.; O'Neill, P.; Goodwin, P. M.; Pennathur, S.; Fygenson, D. K. *Langmuir* **2011**, *27*, 8923–8933.
- (16) Sharma, J.; Yeh, H.-C.; Yoo, H.; Werner, J. H.; Martinez, J. S. *Chem. Commun.* **2010**, *46*, 3280–3282.
- (17) Zheng, L.; Zhang, R. C.; Ni, Y. X.; Du, Q.; Wang, X.; Zhang, J. L.; Li, W. *Catal. Lett.* **2010**, *139*, 145–150.
- (18) Fu, Y.; Zhang, J. L.; Chen, X. F.; Huang, T. T.; Duan, X. L.; Li, W.; Wang, J. K. *J. Phys. Chem. C* **2011**, *115*, 10370–10379.
- (19) Li, T.; Zhang, L.-B.; Ai, J.; Dong, S.-J.; Wang, E.-K. *ACS Nano* **2011**, *5*, 6334–6338.
- (20) Izatt, R. M.; Christensen, J. J.; Rytting, J. H. *Chem. Rev.* **1971**, *71*, 439–481.
- (21) Berti, L.; Burley, G. A. *Nature Nanotechnol.* **2008**, *3*, 81–87.
- (22) Wang, Y.; Ouyang, G. H.; Zhang, J. T.; Wang, Z. Y. *Chem. Commun.* **2010**, *46*, 7912–7914.
- (23) Guo, W. W.; Yuan, J. P.; Wang, E. K. *Chem. Commun.* **2009**, *23*, 3395–3397.
- (24) Sun, L.; Sun, Y.; Xu, F.; Zhang, Y.; Yang, T.; Guo, C.; Liu, Z.; Li, Z. *Nanotechnology* **2009**, *20*, 125502.
- (25) Behrens, S.; Heyman, A.; Maul, R.; Essig, S.; Steigerwald, S.; Quintilla, A.; Wenzel, W.; Bürck, J.; Dgany, O.; Shoseyov, O. *Adv. Mater.* **2009**, *21*, 1–5.
- (26) Mpourmpakis, G.; Caratzoulas, S.; Vlachos, D. G. *Nano Lett.* **2010**, *10*, 3408–3413.
- (27) Schreiber, M.; González, L. *J. Comput. Chem.* **2007**, *28*, 2299–2308.
- (28) Brancolini, G.; Felice, R. D. *J. Phys. Chem. B* **2008**, *112*, 14281–14290.
- (29) Verdugo, V.-S.; Metiu, H.; Gwinn, E. *J. Chem. Phys.* **2010**, *132*, 195102–195110.
- (30) Perdew, J. P.; Wang, Y. *Phys. Rev. B: Condens. Matter.* **1992**, *45*, 13244–13249.
- (31) Perdew, J. P.; Yue, W. *Phys. Rev. B: Condens. Matter.* **1986**, *33*, 8800–8802.
- (32) Snoussi, K.; Halle, B. *Biochem.* **2008**, *47*, 12219–12229.
- (33) Neidle, S. *Oxford Handbook of Nucleic Acid Structure*; Oxford University Press: New York, 1999.
- (34) Li, W.; Miyoshi, D.; Nakano, S.-I.; Sugimoto, N. *Biochem.* **2003**, *42*, 11736–11744.
- (35) Lipps, H. J.; Rhodes, D. *Trends Cell Biol.* **2009**, *19*, 414–422.
- (36) Simonsson, T. *Biol. Chem.* **2001**, *382*, 621–628.
- (37) Li, W.; Wu, P.; Ohmichi, T.; Sugimoto, N. *FEBS Lett.* **2002**, *526*, 77–81.
- (38) Schultze, P.; Hud, N. V.; Smith, F. W.; Feigon, J. *Nucleic Acids Res.* **1999**, *27*, 3018–3028.
- (39) Gaynudinov, T. I.; Neumann, R. D.; Panyutin, I. G. *Nucleic Acids Res.* **2008**, *36*, 4079–4087.
- (40) Setnička, V.; Urbanová, M.; Volka, K.; Nampally, S.; Lehn, J. M. *Chem.—Eur. J.* **2006**, *12*, 8735–8743.
- (41) Setnička, V.; Nový, J.; Böhm, S.; Sreenivasachary, N.; Urbanová, M.; Volka, K. *Langmuir* **2008**, *24*, 7520–7527.
- (42) Van Mourik, T.; Dingley, A. J. *Chem.—Eur. J.* **2005**, *11*, 6064–6079.
- (43) Gu, J.; Leszczynski, J. *J. Phys. Chem. A* **2000**, *104*, 6308–6313.
- (44) Gu, J.; Leszczynski, J. *J. Phys. Chem. A* **2002**, *106*, 529–532.
- (45) Loo, K.; Degtyareva, N.; Park, J.; Sengupta, B.; Reddish, M.; Rogers, C. C.; Bryant, A.; Petty, J. T. *J. Phys. Chem. B* **2010**, *114*, 4320–4326.
- (46) Koszinowski, K.; Ballweg, K. *Chem.—Eur. J.* **2010**, *16*, 3285–3290.
- (47) Guo, W.-W.; Yuan, J.-P.; Dong, Q.-Z.; Wang, E.-K. *J. Am. Chem. Soc.* **2010**, *132*, 932–934.
- (48) Ono, A.; Cao, S.; Togashi, H.; Tashiro, M.; Fujimoto, T.; Machinami, T.; Oda, S.; Miyake, Y.; Okamoto, I.; Tanaka, Y. *Chem. Commun.* **2008**, *39*, 4825–4827.
- (49) Neidig, M. L.; Sharma, J.; Yeh, H.-C.; Martinez, J. S.; Conradson, S. D.; Shreve, A. P. *J. Am. Chem. Soc.* **2011**, *133*, 11837–11839.
- (50) Jamorski, C.; Foresman, J. B.; Thilgen, C.; Lüthi, H.-P. *J. Chem. Phys.* **2002**, *116*, 8761–8771.